Desalination and Water Treatment
www.deswater.com

doi: 10.5004/dwt.2021.27449

231 (2021) 16–26
August

Effect of aeration intensity and aeration pattern on a compact biofilm reactor for rural domestic sewage treatment in China: pollutant removal performance and hydrodynamic behavior

Weiyi Wang[a], Du Guo[a], Tingting Du[a], Ming Zeng[a,*], Chang Wang[a], Nan Wu[b], Zongpeng Zhang[c]

[a]*College of Marine and Environmental Sciences, Tianjin University of Science and Technology, 300457 Tianjin, China, emails: ming.zeng@tust.edu.cn (M. Zeng), 958121760@qq.com (W. Wang), 463634310@qq.com (D. Guo), 1404093761@qq.com (T. Du), wangc88@tust.edu.cn (C. Wang)*
[b]*College of Engineering and Technology, Tianjin Agricultural University, Tianjin 300384, China, email: nwu@tjau.edu.cn*
[c]*Fukai Diwo (Tianjin) Environmental Protection Technology Co., Ltd., 300457 Tianjin, China, email: 489580114@qq.com*

Received 11 March 2021; Accepted 21 May 2021

ABSTRACT

The treatment of rural domestic sewage in China requires a process with low operational cost and easy maintenance. Thus, the effect of aeration intensity and aeration pattern on the treatment effect of bioreactor needs to be well investigated. In this study, the pollutant removal performance and hydrodynamic behavior of a compact biofilm reactor (purification tank) under different aeration conditions were studied. The results show that the gas rising velocity of 0.066 m s^{-1} led to a better pollutant performance and hydrodynamic behavior, compared with the velocity of 0.013 and 0.120 m s^{-1}. Particularly, the increased nitrogen removal efficiency reduced the bubble size and increased turbulence between the gas–liquid phases took place at this medium aeration intensity. Besides, under the multistage A/O pattern with step-feed, the average effluent concentrations of NH_4^+–N and total nitrogen were 3 and 14 mg L^{-1}, respectively, which are lower than national discharge standards of pollutant for municipal wastewater treatment plant (GB18918-2002). The step-feed operation in the second anaerobic zone of the purification tank could well solve the problem of insufficient carbon source, and strengthen the nitrogen removal function. Overall, the experimental study and hydrodynamic modeling provide the direction for the application of a full-scale purification tank in rural China.

Keywords: Biological wastewater treatment; Domestic sewage; Rural China; Purification tank; Computational fluid dynamics

1. Introduction

In 2010, the population of China's rural areas has reached 660 million [1]. The daily discharge of domestic sewage has reached more than 30 million tons, and the ratio of treated rural domestic sewage is only 7% [2]. The organic matter, nitrogen, phosphorus, and other pollutants in this domestic sewage seriously threaten the rural ecological environment security, because of the lack of investment and people's weak awareness of environmental protection. Due to the imbalance development of rural areas in China, the emission of wastewater and the concentration of pollutants vary greatly. Hou et al. [3] summarized the data of rural domestic sewage of 11 provinces and cities in China and reported that the emission fluctuated in the range of 15 and 116 L (person d)$^{-1}$, with an average value

* Corresponding author.

of 60 L (person d)$^{-1}$. The chemical oxygen demand (COD), total nitrogen (TN) and total phosphorus varied from 62 to 1,200 mg L^{-1}, 11 to 151 mg L^{-1} and 0.3 to 14 mg L^{-1}, respectively.

Thus, rural domestic sewage has the characteristics of scattered discharge sources, large fluctuation of water quality and quantity, etc. Therefore, the decentralized treatment process with low operational cost and easy maintenance should be selected for the treatment of rural sewage [4,5]. As a compact biofilm reactor, the purification tank is a very suitable technology for in-situ treatment of rural domestic sewage, which has the advantages of good impact resistance, solid–liquid separation and simple installation. This technology has become a new concept of domestic sewage treatment [6,7].

The effect of aeration intensity and aeration pattern on the treatment effect of bioreactor is particularly significant. The aeration intensity is represented by the air-flow rate, which is not only one of the important limiting factors of microbial activity, but also one of the vital energy consumption indicators of domestic sewage treatment. Because the purification tank is for decentralized rural domestic sewage treatment, it makes sense to control the aeration rate to save the operation cost. Besides, the aeration pattern has a great influence on the removal of nitrogen in domestic sewage treatment [8]. At present, the purification tank can effectively remove organic matter [9]. In order to prevent the occurrence of eutrophication, nitrogen removal of rural domestic sewage is needed to be considered, but there is quite a little research on this aspect. Compared with the traditional A^2/O process, the multistage A/O process has the advantage of low energy consumption [10]. At present, there is no report about the application of the multistage A/O process in the purification tank.

The computational fluid dynamics (CFD) method has been demonstrated to be a useful tool for understanding flow behavior with short analyzing time compared with experiments [11]. Two main approaches are used in CFD: the Eulerian approach that regards the dispersed phase as interpenetrating continua, and the Lagrangian approach that treats the dispersed phase as discrete entities [12–14]. Díez et al. [15] established CFD models to investigate the multiphase flow in sequencing batch reactor (SBR) by means of hybrid methods. Kulisiewicz et al. [16] employed a coupled experimental and numerical approach to investigate the granulation process of activated sludge in the biological purification of wastewater in SBR. Wang et al. [17] applied CFD to simulate hydrodynamics information in an expanded granular sludge bed reactor used for biohydrogen production. Ren et al. [18] aimed at developing hydraulic and CFD models to describe the hydrodynamics of the up-flow anaerobic sludge blanket reactors. These results show that CFD is more and more widely used in analyzing the characteristics of bioreactor. Thus, CFD can be used to predict the change of the flow pattern in the purification tank, so as to optimize the air-flow rate and aeration pattern in the purification tank.

Effects aeration intensity and aeration pattern on the removal of various pollutants were studied by experimental means. Specifically, the removal performance of pollutants under three different gas rising velocities was compared, and the nitrogen removal effect under the multistage A/O process was investigated. On the other hand, the 3-D transient gas–liquid two-phase flow CFD model was established to describe the hydrodynamic characteristics of the purification tank at different gas rising velocities. These studies provide a reference for the practical application of the purification tank in treating rural domestic sewage in China.

2. Methods and materials

2.1. Set-up of bioreactor

According to the treating efficiency, there exist two types of purification tanks: a tank for a single household (anaerobic and aerobic pattern) and a tank for advanced nitrogen removal (multistage A/O pattern). The purification tank for a single household was designed to treat the sewage from 5 people's households, as shown in Fig. 1a, consisted of two anaerobic zones and one aerobic zone. The volume in the primary anaerobic zone, secondly anaerobic zone, aerobic zone and settling zone were 14.5, 12.5, 11.5 and 5.0 L, respectively. The lab-scale tank for advanced nitrogen removal, as shown in Fig. 1b, consisted of two anaerobic zones and two aerobic zones with 10 L for each zone.

To increase the surface, strength and corrosion resistance of the biofilm in the purification tank, a porous corrugated plate was used as the biofilm carrier with a specific surface area of 70 m^2 m^{-3} and a filling volume of 60% of each zone. Wastewater gravely flew from inlet to outlet in the bioreactor, because the static pressure difference was kept in an

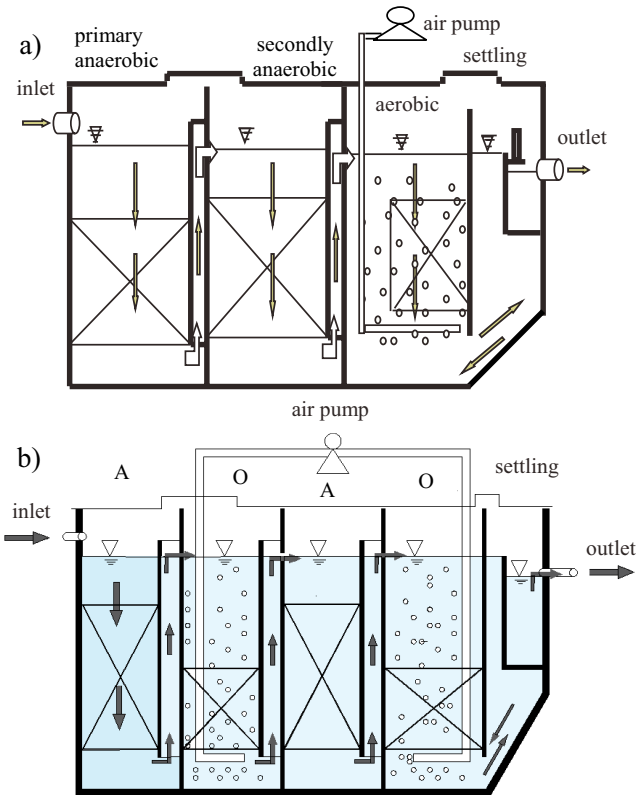

Fig. 1. Schematic diagram of lab-scale purification tank for single household (a) and advanced nitrogen removal (b).

anaerobic zone. There was no back-mixing between different zones. The volume of lab-scale experimental equipment is 1/66 that of the full-scale purification tank.

2.2. Operation of bioreactor

Before the operation of the bioreactor, the formation of aerobic and anaerobic biofilm was firstly performed. For aerobic biofilm, the activated sludge from a wastewater treatment plant in Tianjin was put into the aerobic zone of purifying tank with continuous aeration. One-third of the supernatant was replaced with a feeding solution (component shown in Table 1) each day. After about a week, the brown aerobic biofilm on the surface of the porous corrugated plate was basically formed. Meanwhile, the anaerobic biofilm was formed by immersing the porous corrugated plate in the anaerobic zone of purifying tank. The sewage from Teda Campus of Tianjin University of Science and Technology was fed in an anaerobic zone and one-third of the supernatant was replaced with a feeding solution each day. After about one month, uniform black anaerobic biofilm was formed on the surface of the corrugated plate.

After the biofilm was formed, the real domestic sewage was fed into the tank for a single household and the tank for the advanced nitrogen removal separately. In terms of the purification tank for a single household, three gas rising velocities were successively compared (0, 0.013, 0.066 and 0.120 m s^{-1}) in bioreactors, which were calculated by dividing the gas flow rate by the surface area of each zone. The continuous water feeding was adopted with a water flow rate of 15 L d^{-1}, so the hydraulic retention time for the primary anaerobic zone, secondly anaerobic zone and aerobic zone, settling zone was 23, 20, 18 and 8 h, respectively. The water temperature was room temperature ranging between 20°C and 25°C. The influent domestic sewage was collected from the Teda Campus of Tianjin University of Science and Technology. The average water quality indexes of domestic sewage are shown in Table 1. The operating period for each gas rising velocity lasted for one week. The water quality of each zone in the purification tank was daily sampled and analyzed.

After the gas rising velocity was fixed, the purification tank for the advanced nitrogen removal was designed for the rural region that needs the requirement for the strict discharged nitrogen content. The first and third zones belonged to the anaerobic zone and the second and fourth zones were aerobic zones. Each zone owned the same volume of 10 L. The gas rising velocity was controlled to be 0.066 m s^{-1}. The influent domestic sewage was collected from the Teda Campus of Tianjin University of Science and Technology (Table 1). The continuous water feeding was adopted with a water flow rate of 15 L d^{-1} for three weeks. Then, in order to enhance the nitrogen removal efficiency, the step-feed operation was conducted that two parts of influent were separately pumped into first and secondary anaerobic zones at a ratio of 2:1 for three weeks. The water quality of each zone in the purification tank was daily sampled and analyzed.

Table 1
Influent quality parameters of real domestic sewage used in the experiment

Parameters	Tank for single household	Tank for the advanced nitrogen removal
COD (mg L^{-1})	376.3	316.4
BOD_5 (mg L^{-1})	228.9	155.0
Turbidity (NTU)	138.3	61.2
pH	7.3	7.9
NH_3–N (mg L^{-1})	48.7	61.7
NO_3^-N (mg L^{-1})	2.1	0.2
TN (mg L^{-1})	–	85.5
Temperature (°C)	17–22	16–23

2.3. Physicochemical analysis

Dissolved oxygen (DO) was measured using a DO meter (850A, Thermo Electron Co., USA). Turbidity was analyzed using a turbidity meter (AQ2010, Thermo Electron Co., USA). Biochemical oxygen demand (BOD_5) was determined using BOD detecting instrument (CY-II, Guangdong Medical Appliance Co., China) and COD was measured using a COD analytical instrument (COD-571, Shanghai Precision Scientific Instrument Co., China).

2.4. CFD mathematical model

2.4.1. Model geometry and computational mesh

The geometry of the lab-scale purification tank was set to be the length of 0.526 m, the width of 0.406 m and the height of 0.405 m. A total of 15 aerators were set, evenly distributed at the bottom of the purification tank. The top of the reactor was believed to be an air outlet. A schematic of the lab-scale purification reactor and its computational meshes for the 2D and 3D geometries are shown in Fig. 2.

Both geometries were created in ANSYS®-Design Modeler and the meshes were established in ANSYS®-Meshing. Computational meshes comprised of quadrilateral and triangular elements were built, for the 3D model. A total of 354,497 nodes and 240,239 grids were set up as shown in Fig. 2b.

2.4.2. Eulerian-Eulerian model

FLUENT software offers 4 models of multiphase flow: VOF model, mixture model, Eulerian model and wet steam model. The VOF model, mixture model and Eulerian model all belong to Eulerian calculation methods for dealing with multiphase flows. Compared with the VOF model, the mixture model and Euler model are suitable for the calculation of gas–liquid two-phase flow with volume concentration greater than 10%. Considering the accuracy of the model, the Euler model was selected in this study.

In the simulation, the mixing of gas–liquid two-phase flow in the purification tank was analyzed. The deformation of a single bubble and the fragmentation and coalescence of multiple bubbles were not considered. The bubbles were assumed to be rigid spheres, and there was no interaction between particles. In this study, a transient CFD model

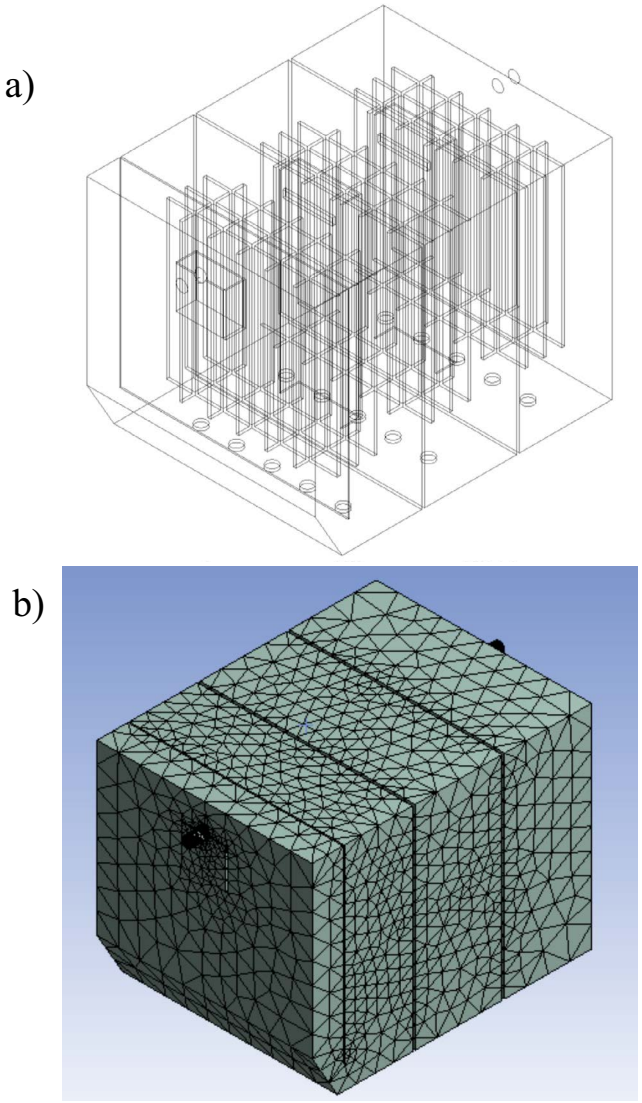

Fig. 2. Three-dimensional computational domain: (a) reactor schematic diagram and (b) computational grid.

was adopted, in which water was set as the primary phase and gas as the secondary phase.

2.4.3. Governing equations

For gas–liquid two-phase flow, the two-fluid model assumes that each phase in the two-phase flow field is a continuous medium. Two phases of gas and liquid are full of the whole flow field at the same time. The flow parameters of each phase are discontinuous on the phase interface. There are mass, momentum and energy equations between phases on the interface Eqs. (1)–(3), as well as the supplementary equations of phase interface heat transfer, mass transfer equation, interface stress equation, physical equation and thermodynamics state equation.

Continuity equation:

$$\frac{\partial \rho_k}{\partial t} + \nabla\left(\rho_k u_k\right) = 0 \tag{1}$$

Momentum equation:

$$\frac{\partial \rho_k u_k}{\partial t} + \nabla\left(\rho_k u_k u_k\right) = -\nabla\left(P_k I - T_k\right) + \rho_k g_k = -\nabla\left(P_k I\right) + \nabla T_k + \rho_k g_k \tag{2}$$

Energy equation:

$$\frac{\partial \rho_k}{\partial t}\left(e_k + \frac{u_k}{2}\right) + \nabla\left[\rho_k\left(e_k + \frac{u_k^2}{2}\right)u_k\right] = -\nabla q_k + \nabla\left[\left(-P_k I + T_k\right)u_k\right] + \rho_k g_k u_k \tag{3}$$

where the angular code representing the phase ($k = g$ represents the gas phase here, $k = l$ represents the liquid phase), and u_k represents the velocity vector of each phase. P_k is the pressure scalar of each phase; I is the unit tensor; T is the shear stress tensor; g_k is the acceleration vector of gravity; e_k is specific internal energy.

2.4.4. Solver settings

Due to the complex flow patterns in the purification tank, the standard k-ε turbulence model was chosen. The experiment adopted Euler multiphase flow mathematical model. The set of governing equations for the 3D unsteady models was solved with the finite volume method, performing a pressure-velocity coupling and using the phase-coupled SIMPLE algorithm. The turbulent kinetic energy adopted the first-order upwind scheme, the gradient adopted the least-squares cell-based scheme, and the pressure interpolation adopts the PRESTO! scheme and the momentum and volume Fraction were discretized using the QUICK scheme. A convergence criterion of 10^{-3} (relative error) for all scaled residuals was established.

3. Results

3.1. Effects of gas velocity on pollutant removal performance

3.1.1. Organic matter removal performance

The changes of COD in each zone of the purification tank under different gas rising velocities in the aerobic tank are shown in Fig. 3a. Since two anaerobic zones had the pre-treatment function for COD degradation, for example, the macromolecular particulate matter being hydrolysis fermented, the COD removal efficiency by the first two anaerobic zones was about 65% with effluent COD of 110 ± 6 mg L^{-1} for the subsequent zone. Moreover, it can be found that the COD removal was still weak when the subsequent zone was in an anaerobic condition (Fig. 3a).

Once the aeration was introduced, it can be seen that the COD degradation ability was continuously increased along with the augmentation of aeration intensity. Specifically, COD was slightly degraded to 84 mg L^{-1} at the gas rising velocity of 0.013 m s^{-1}, however it was greatly removed at the air velocity of 0.066 m s^{-1} with an effluent COD concentration of 41 mg L^{-1}. Finally, it is indicated the larger air velocity of 0.120 m s^{-1} cannot greatly contribute to the higher removed COD amount.

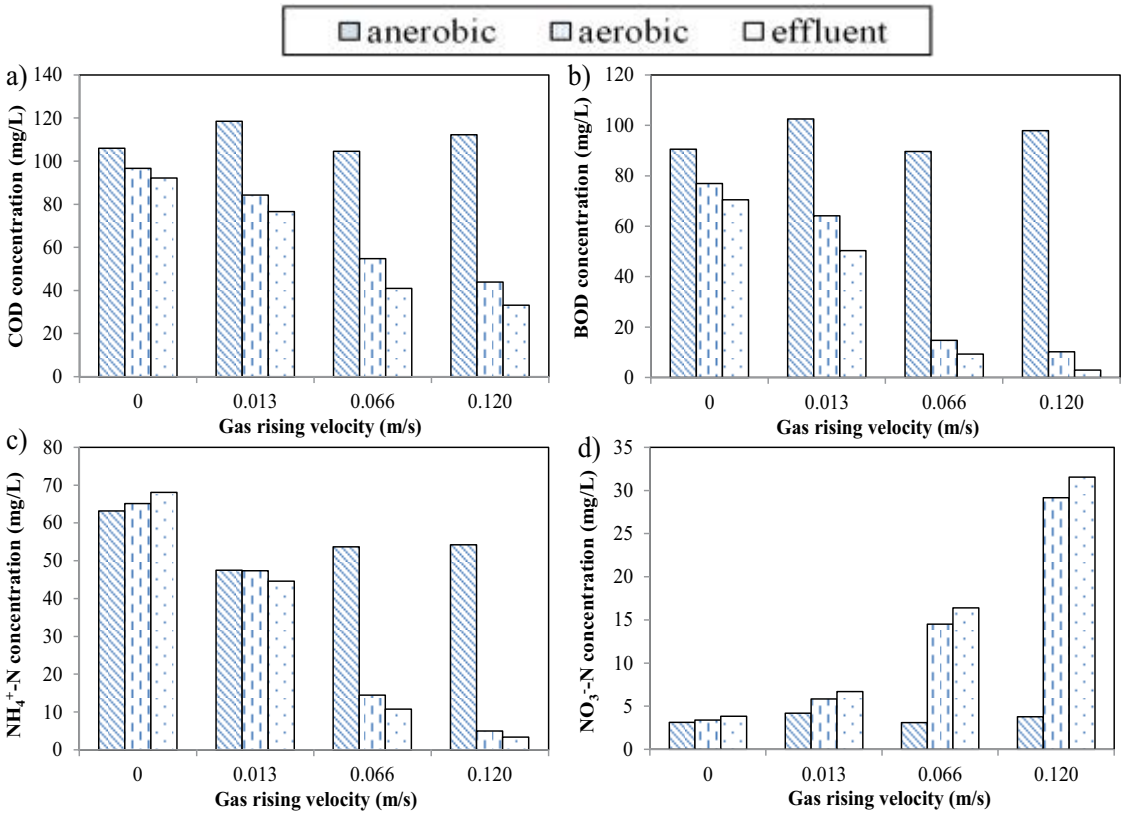

Fig. 3. Changes of COD (a), BOD_5 (b), NH_4^+–N (c) and NO_3^-–N (d) concentrations in different zones of purification tank under three gas rising velocities.

The BOD_5 changes of each zone in the purification tank under different gas rising velocities were shown in Fig. 3b. The changing trend of BOD_5 was similar to that of COD. Along with the increase of gas rising velocity in the aerobic tank, effluent BOD_5 concentration dropped rapidly, when the gas rising velocity of aeration increased to 0.066 m s^{-1}, the dissolved oxygen concentration in the aerobic tank reached 3.15 mg L^{-1} and effluent BOD_5 arrived at 9 mg L^{-1}, meeting discharge standards of pollutant for municipal wastewater treatment plant [19]. Subsequently, due to the limitation of biological treatment technique, the BOD_5 could not be greatly degraded although the increase of gas rising velocity up to 0.120 m s^{-1}.

3.1.2. Nitrogen removal performance

The effects of aeration intensity on the NO_3^-–N and NH_4^+–N concentrations were shown in Fig. 3c and d. The anaerobic condition did not change the nitrogen concentration. Along with the increase of gas rising velocity in the aerobic zone, the effluent NH_4^+–N concentration was greatly reduced. Specifically, when the gas rising velocity reached 0.066 m s^{-1} in the aerobic zone, the NH_4^+ removal efficiency reached 80% with the effluent NH_4^+–N concentration of 11 mg L^{-1}. The higher gas rising velocity of 0.120 m s^{-1} further increased NH_4^+ removal efficiency to 94% with the effluent NH_4^+–N concentration being 3 mg L^{-1}.

Accompanied by the decrease of NH_4^+, the NO_3^-–N concentration correspondingly increased, especially up to 16 and 32 mg L^{-1} at high gas rising velocities of 0.066 and 0.120 m s^{-1} (Fig. 3d). The difference of reduced NH_4^+–N and produced NO_3^-–N concentration was calculated to be 30 and 23 mg L^{-1} at gas rising velocity of 0.066 and 0.120 m s^{-1}, respectively. This means that more NH_4^+ was removed at the gas rising velocity of 0.066 m s^{-1}.

3.2. Effects of aeration pattern on pollutant removal performance

3.2.1. Removal performance of multistage A/O pattern

Fig. 4 shows the change of COD concentration in different zones of the purification tank under a multistage A/O pattern. The first anaerobic reaction zone (A1) contributed to the COD removal efficiency of 34% and 38% at 6 and 21 d, respectively. Then the first aerobic reaction zone (O1) further increased the COD removal efficiency to 82% and 86% at 6 and 21 d, respectively. After these two zones, the COD concentration did not significantly change. Finally, the effluent COD concentration reached 20 and 18 mg L^{-1} at 6 and 21 d, respectively, which is far lower than 50 mg L^{-1} in the national standard (GB18918-2002). Compared with the former anaerobic–aerobic pattern, the multistage A/O pattern with an aerobic process maintained a high COD treating efficiency.

Fig. 4b–d shows the concentration changes of NH_4^+–N, NO_3^-–N and TN in the different zones of the purification tank under a multistage A/O pattern. It can be seen that the first anaerobic zone (A1) did not greatly change nitrogen

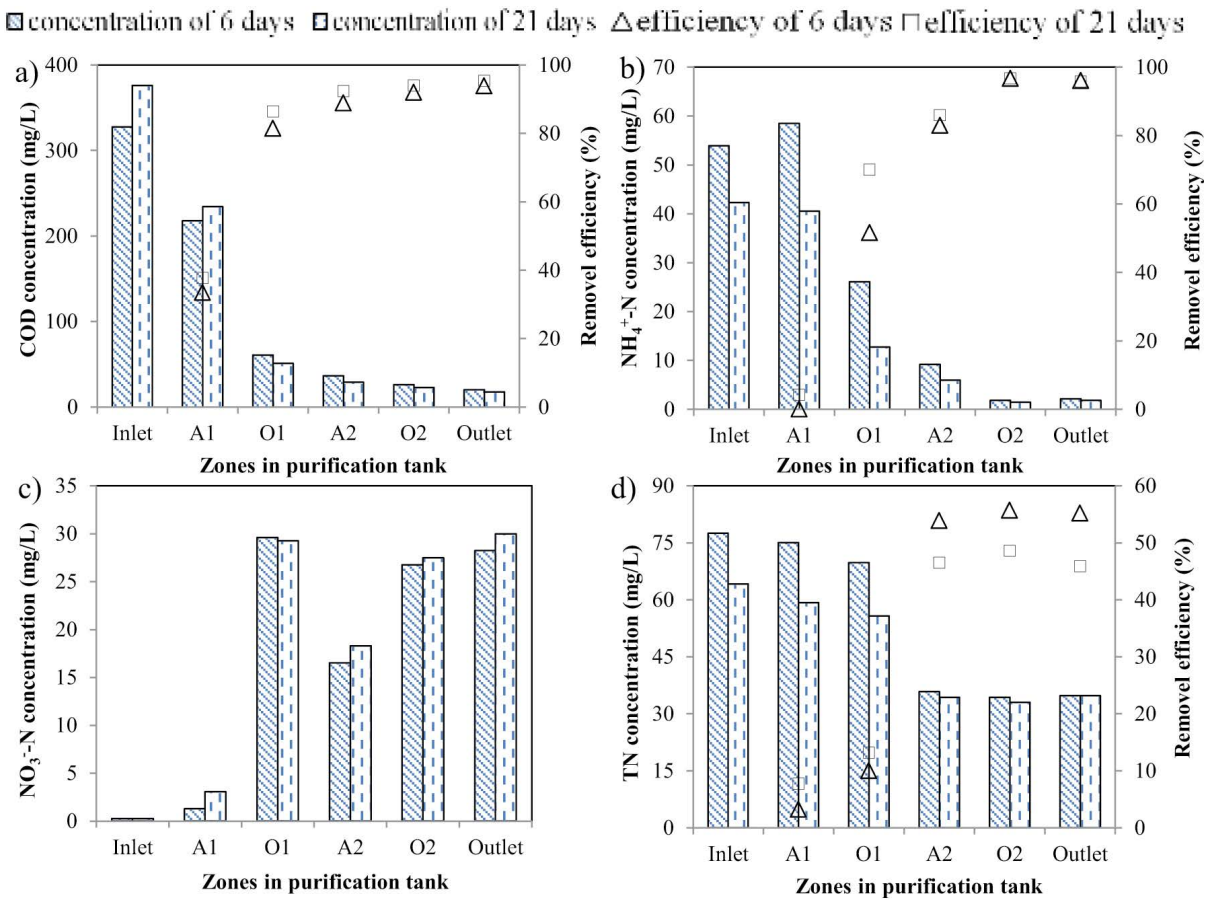

Fig. 4. Change of COD (a), NH_4^+–N (b), NO_3^-–N (c) and TN (d) concentration and their removal efficiencies in different zones of purification tank under multi-stage A/O mode.

concentration. After the first aerobic zone (O1), the average NH_4^+–N concentration decreased to 20.9 mg L^{-1}, while the average NO_3^-–N concentration increased up to 30.5 mg L^{-1}, and the concentration of TN slightly changed. After the secondary anaerobic reaction zone (A2), the average NO_3^-–N concentration decreased to 19.3 mg L^{-1}, and the TN concentration decreased to 36.4 mg L^{-1}, which was caused by the denitrification process. Finally, and the average effluent NH_4^+–N concentration arrived at 2 mg L^{-1}, which was lower than the discharge standards of pollutant for municipal wastewater treatment plant (GB18918-2002), and its average removal efficiency reached 95%. However, the average effluent NO_3^-–N concentration (30.3 mg L^{-1}) and TN concentration (34.9 mg L^{-1}) was relatively high due to the lack of carbon sources in the wastewater from the second anaerobic zone. Therefore, it is very necessary to provide carbon sources for the advanced nitrogen removal process.

3.2.2. Removal performance of multistage A/O pattern with step-feed

Fig. 5 shows the time variation of COD concentration and its removal efficiency in each zone under multistage A/O pattern with step-feed. It can be observed that most COD content decreased at the first A1, its removal efficiency reaching 81% and 84% at 6 and 21 d (Fig. 5a). The effect of the subsequent second stage A/O was not obvious. The step-feed operation was not found to stimulate the increase of COD in the second anaerobic zone, which means that it can be strongly used by the biofilm in this zone. Finally, the effluent COD concentration was reduced to about 12 mg L^{-1} with the COD removal efficiency of around 95%.

Fig. 5b–d shows the concentration changes of NH_4^+–N, NO_3^-–N and TN in each reaction zone of the purification tank multistage A/O pattern with step-feed. It can be observed that the nitrogen removal performance of the first A1 and O1 zones was strengthened. After the first O1 zone, the NH_4^+–N and TN removal efficiency reached 77% and 25% after 6 d, which was great larger than those without step-feed. Besides, this stable nitrogen removal performance could be maintained after 21 d. Moreover, due to the carbon source provided into the A2 anaerobic zone, the nitrogen removal efficiency was enhanced. The concentrations of NO_3^-–N and TN further decreased, and the average concentrations of NH_4^+–N, NO_3^-–N and TN were 3, 11 and 14 mg L^{-1}, respectively, which are all lower than the discharge standards of pollutant for municipal wastewater treatment plant (GB18918-2002). It can be concluded that the step-feed operation in the second anaerobic zone of the purification tank can well solve the problem of insufficient carbon source, and strengthen the nitrogen removal function.

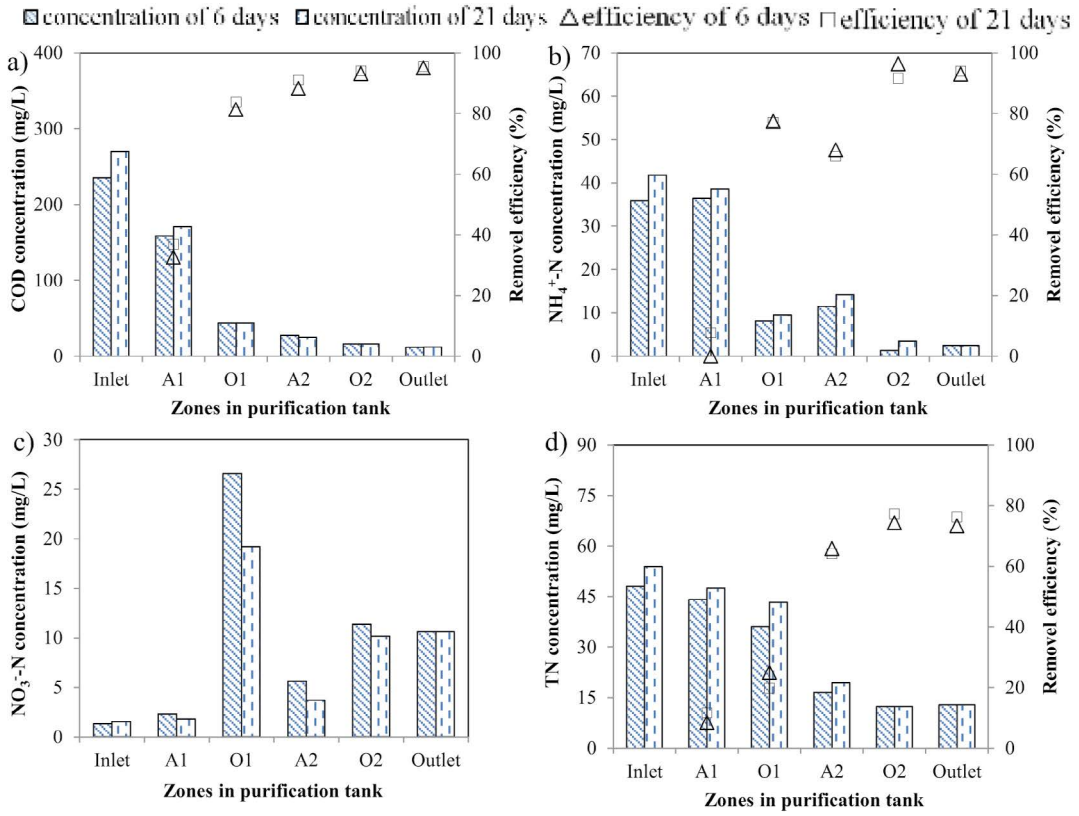

Fig. 5. Change of COD (a), NH_4^+–N (b), NO_3^-–N (c) and TN (d) concentration and their removal efficiencies in each zone under multi-stage A/O mode with step-feed.

3.3. Visualization of the flow pattern under different gas rising velocities

3.3.1. Gas velocity distribution

In this simulation, a lab-scale purification tank for a single household was used as the research object to evaluate the flow pattern under different gas rising velocities. The gas-phase velocity vector diagram under different aeration velocities in the whole purification tank is shown in Fig. 6. Air bubbles between the aerator and the bottom of the biofilm carrier tended to be in a divergent state under the aeration condition. Specifically, it can be seen that the gas distribution started to be uniform at the gas rising velocity of 0.066 m s^{-1}. Therefore, the divergence started to be uniform, being beneficial to increase the contact of gas–liquid phases. When the bubbles passed through the packing area, they were blocked and cut by the biofilm carrier, resulting in the breaking of large bubbles, increasing the gas–liquid contact area and improving the oxygen transfer efficiency. In the experiment, when the rising velocity of dissolved oxygen in wastewater was 0.066 m s^{-1}, the DO concentration increased to be 3 mg L^{-1}. When the rising velocity increased to 0.120 m s^{-1}, the gas velocity vector graph was similar to that at 0.066 m s^{-1}.

3.3.2. Liquid flow field

The liquid phase flow field in the purification tank with different gas rising velocities is shown in Fig. 7. In the process of simulation, the main influence factor of the liquid flow field is the disturbance in the process of bubbles rising inside of biofilm carrier. As the top surface of the purification tank is set as the escape exit, only the gas phase can escape. Therefore, when the liquid phase was brought to the top surface by bubbles, it will fall back under the action of gravity and form reflux between the aerator and water surface.

By comparing the flow charts under different gas rising velocities, when there was no aeration in the tank, a breakpoint appeared in the flow chart inside the biofilm carrier, indicating that the liquid phase distribution was not uniform. When the gas rising velocity arrived at 0.013 m s^{-1}, the flow uniformity became better, but no eddy current was formed. Furthermore, when the gas velocity further increased to 0.066 m s^{-1}, the fluid in the purification tank had the best hydrodynamic behavior being uniform. This phenomenon indicates that the gas velocity in the purification tank played an important role in the flow field distribution in the tank. The velocity of 0.120 m s^{-1} contributed to a smaller vortex at the top of the purification tank relative to the velocity of 0.066 m s^{-1}. This is probably because the excessive gas rising flow velocity gave a strong shock to the liquid flow, which made the vortex smaller that could not be observed at the bottom of the packing. Since the vortex at the bottom of the biofilm carrier was more favorable for the renewal of the biofilm attached to the carrier, so the gas rising velocity of 0.066 m s^{-1} was suggested to be adopted.

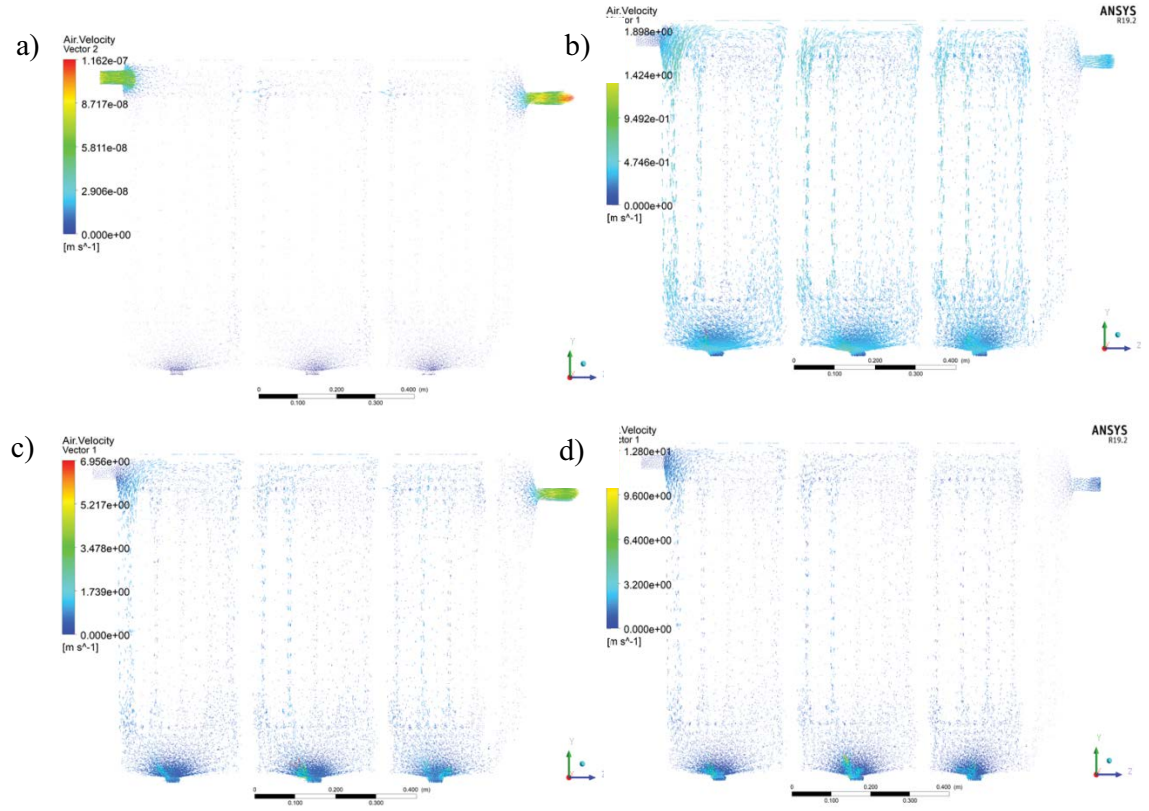

Fig. 6. The gas-phase velocity vector diagram under anaerobic condition (a) and aerobic condition with gas rising velocities of 0.013 m s^{-1} (b), 0.066 m s^{-1} (c) and 0.120 m s^{-1} (d).

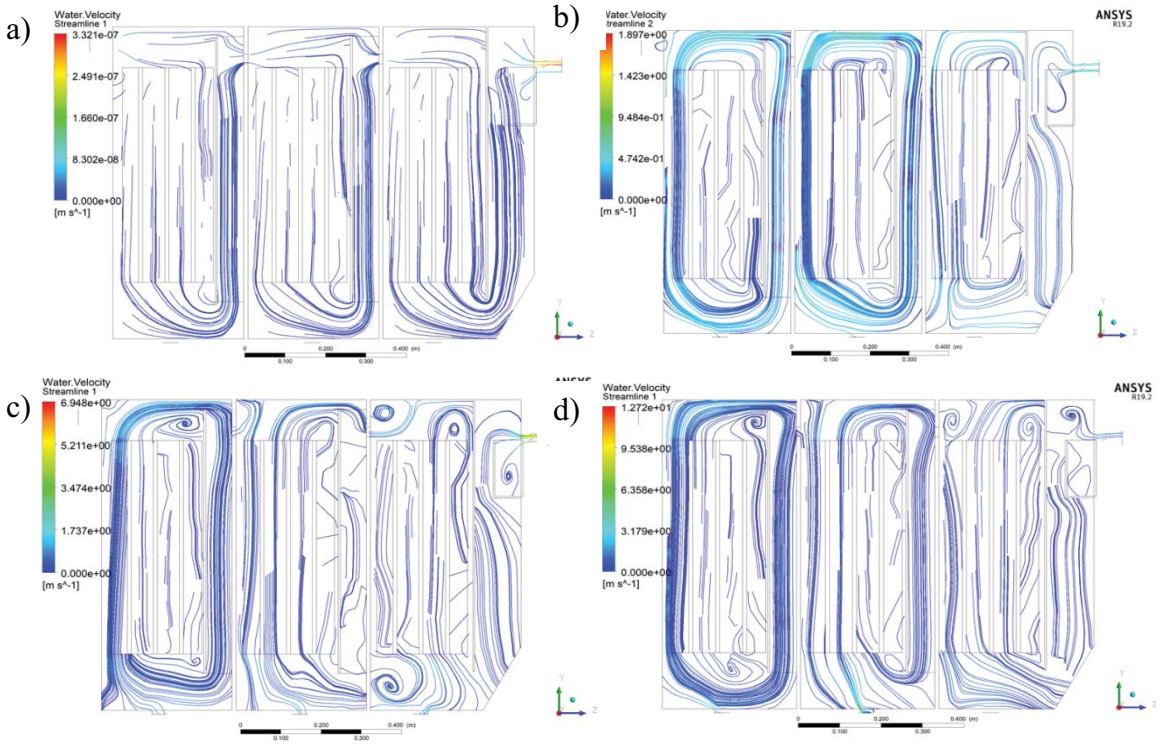

Fig. 7. The liquid flow field diagram under anaerobic condition (a) and aerobic condition with gas rising velocities of 0.013 m s^{-1} (b), 0.066 m s^{-1} (c) and 0.120 m s^{-1} (d).

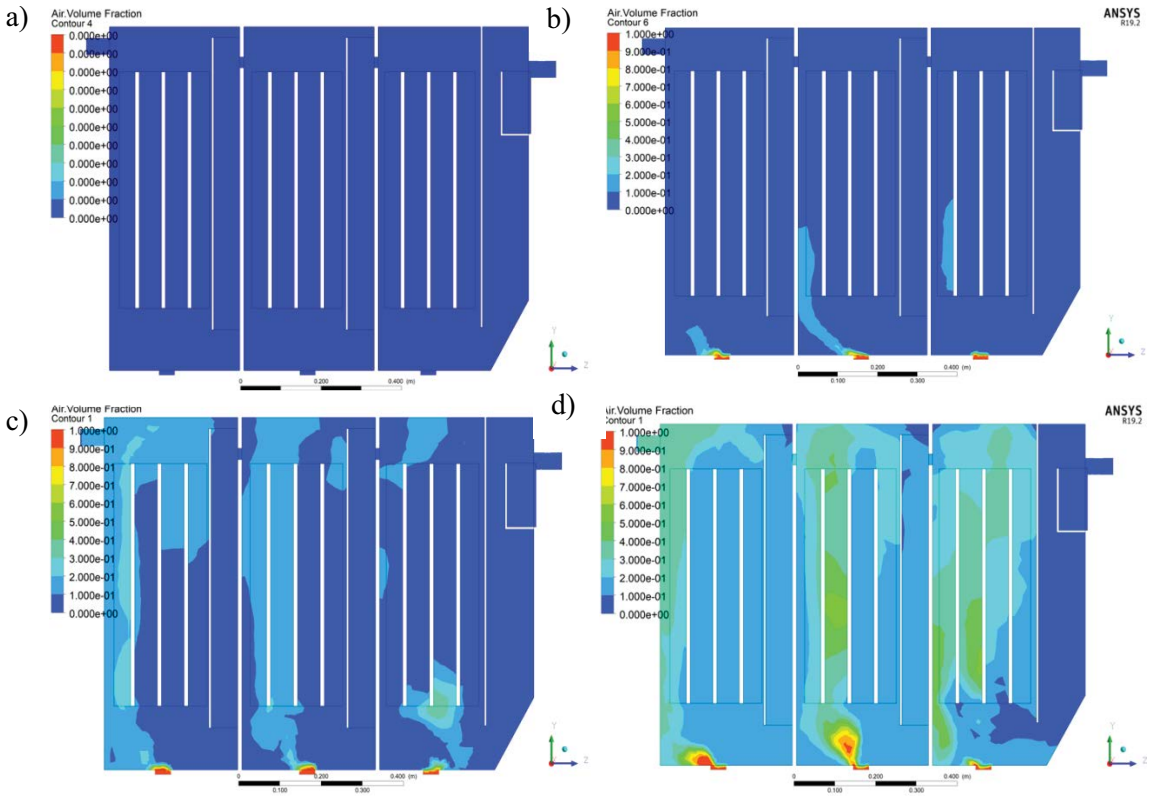

Fig. 8. The cloud chart of gas content distribution under anaerobic condition (a) and aerobic condition with gas rising velocities of 0.013 m s^{-1} (b), 0.066 m s^{-1} (c) and 0.120 m s^{-1} (d).

3.3.3. Gas content

The distribution of gas content under different gas rising velocities is shown in Fig. 8. Along with the increase of gas rising velocity, the gas phase distribution from the aerator on the cross-section was more extensive, and the gas content was higher. It is found that when the gas rising velocity reached 0.013 m s^{-1}, the gas content was small and there was no obvious gas distribution above the biofilm carrier. However, when the gas rising velocity increased up to 0.066 m s^{-1}, the gas phase could pass through the whole biofilm carrier and appear at the top of the purification tank. Finally, the largest gas rising velocity of 0.120 m s^{-1} allowed the gas to be distributed to the whole system, which might possess the strong shear force to the biofilm on the surface of the carrier. Shortly, appropriately increasing the rising velocity can not only reduce the bubble size and increase the turbulence between the two phases but also shorten the saturation time of the gas phase.

By analyzing the flow field and gas content distribution of gas–liquid two phases, it is concluded that the optimum gas rising velocity was 0.066 m s^{-1}. At this velocity, the bubble diverges most evenly between the aerator and the bottom of the biofilm carrier, which was conducive to increasing the contact time of gas–liquid two phases and improving the oxygen transfer efficiency. Besides, at this medium velocity, the uniformity of the fluid in the purification tank was the best, and the vortex formed by the liquid phase was more favorable for the renewal of the biofilm attached to the biofilm carrier.

4. Discussion

The gas rising velocity that was controlled by the aeration intensity determined the operational cost of the bioreactor. First, the aerobic condition is necessary to be used in rural sewage treatment to reach the discharge standards of pollutant for municipal wastewater treatment plant (GB18918-2002). For example, in our study, although pollutants in sewage were treated by two-stage anaerobic condition via fermentation and hydrolysis, the secondary anaerobic effluent BOD_5 was still higher than the standard limit of 30 mg L^{-1} and needed to be further degraded.

Furthermore, the aeration intensity should be set at an appropriate level. It is reported that the low velocity of 0.013 m s^{-1} was not enough to give a high removal efficiency of COD and NH_3, and the velocity of 0.120 m s^{-1} was too high for the pollutant removal. Most of the pollutant (COD and TN) was biodegraded at the medium gas rising velocity of 0.066 m s^{-1}. For instance, when the gas rising velocity increased to 0.120 m s^{-1}, the NH_3–N removal rate slowed down due to the limitation of the nitrifying bacteria concentration and the hydraulic residence time. However, some researches indicate that low gas velocity can still bring out the high pollutant removal efficiency. For example, the up-flow gas velocity was maintained constant at 0.02 m s^{-1} in the study of Lochmatter et al. [20], where aeration strategies promoted alternating nitrification and denitrification to improve reactor efficiencies of COD, nitrogen and phosphate. Unlike our study, the low gas rising velocity in their study still contributed to the good treating efficiency,

probably due to the suspended sludge in their study rather than the biofilm in our study. As we know, the mass transfer resistance of biofilm for DO requires a higher aeration rate than suspended sludge, so the average DO concentration can be as high as 2.0 ± 1.16 mg L^{-1} in a biofilm reactor, still with a high and stable mean nitrogen removal rate of 0.35 ± 0.19 kg N $(m^3\ d)^{-1}$ [21].

Regarding the hydrodynamic behavior, the gas rising velocity also played an important role. Firstly, bubbles produced by aeration gather near the aerator and are cut and evenly distributed in the whole tank with the help of a biofilm carrier. But the weak aeration with a gas rising velocity of 0.013 m s^{-1} did not make a strong positive effect on the hydrodynamic behavior. Specifically, the gas content was small and there was no obvious gas distribution above the biofilm carrier. This is because the low gas velocity was not enough to make the intense turbulent. Besides, the bubble size was relatively large, not conducive to the contact and mass transfer of gas–liquid two phases. When the gas rising velocity increased up to 0.066 m s^{-1}, the gas phase could pass through the biofilm carrier. Overall, appropriately increasing the rising velocity can not only reduce the bubble size, but also increase the turbulence between the two phases.

Other researchers also reported the positive effect of gas rising velocity on the hydraulic behavior of bioreactor. The gas hold-up and overall oxygen transfer coefficient for all the fluids were found to be increased with the augmentation of gas rising velocity, because the high gas rising velocity contributed to the elevated specific interfacial area with surface tension and bubble size reduction [22]. Devi and Kumar [23] analyzed the flow hydrodynamics and mass transfer mechanisms in a gas–liquid phase bioreactor with wide gas rising velocity range of 0.0075–0.25 m s^{-1}. The volume-averaged velocity magnitude and dissipation rate were found to increase with the augmentation of superficial gas velocity.

In terms of aeration pattern, the multistage A/O process was found to be superior to the anaerobic-aerobic pattern in a traditional purification tank. Furthermore, the step-feed operation was able to realize the advanced nitrogen removal by reasonable assignment of influent carbon source. Specifically, the step-feed allowed the nitrogen removal function of the second anaerobic zone to still being strong. This phenomenon has been reported in other studies [24]. Wang et al. [25] studied a novel four-stage step-feed reactor combined with a fluidized bed, where the NH_4^+–N removal efficiency was 95.7% with the effluent NH_4^+–N concentration less than 8 mg L^{-1}. The study of Zhu et al. [26] showed that high TN removal efficiency (more than 95%) could be achieved under an influent flow rate distribution ratio of 4 avoiding the internal nitrate cycle or addition of an external carbon source.

5. Conclusions

The pollutant removal efficiency of the purification tank could be considerably enhanced with an increase in aeration intensity. But the gas rising velocity was suggested to be controlled at a medium level of 0.066 m s^{-1}. The pollutant removal and hydrodynamic behavior both performed well under this aeration intensity. Besides, appropriately increasing the gas rising velocity could not only reduce the bubble size, but also increased the turbulence between the gas–liquid phases. For the region having a strict requirement for the advanced nitrogen removal, the multistage A/O pattern with step-feed was proposed to conduct, solving the problem of insufficient carbon source and strengthening the nitrogen removal function.

Acknowledgment

This research was financially supported by Tianjin Agricultural Commission Program (201901260), National Undergraduate Training Programs for Innovation and Entrepreneurship (202010057170).

References

[1] C.O.o.t.S. Council, Census Data of China in 2010, China Statistics Press, China, 2012.
[2] J.Y. Ma, J.Y. Zhan, Status of rural domestic sewage treatment in Zhejiang Province, Environ. Sci. Manage., 41 (2016) 64–68 (in Chinese).
[3] J.W. Hou, B. Fan, B. Qu, L. Cai, S.K. Zhu, Review about characteristics of rural domestic wastewater discharge, J. Anhui Agric. Sci., 40 (2012) 964–967 (in Chinese).
[4] G.Q. Wu, X.Y. Sun, Q.S. Zhang, Applicationof purification tank in distributed rural sewage treatment in China, Environ. Sci. Technol., 23 (2010) 36–40 (in Chinese).
[5] X. Feng, J. Zhao, X.M. Lang, X.C. Shi, J.C. Wang, Application prospect of Johkasou to the treatment of rural sewage in China, J. Anhui Agric. Sci., 39 (2011) 4165–4166 (in Chinese).
[6] P. Jin, Y.Y. Chen, T. Xu, Z.W. Cui, Z.W. Zheng, Efficient nitrogen removal by simultaneous heterotrophic nitrifying-aerobic denitrifying bacterium in a purification tank bioreactor amended with two-stage dissolved oxygen control, Bioresour. Technol., 281 (2019) 392–400.
[7] T. Sankai, G. Ding, N. Emori, S. Kitamura, K. Katada, A. Koshio, T. Maruyama, K. Kudo, Y. Inamori, Treatment of domestic wastewater mixed with crushed garbage and garbage washing water by advanced Gappei-Shori Johkaso, Water Sci. Technol., 36 (1997) 175–182.
[8] N.T. Jenzura, A.C. Wendling, A. Zielinski, R.Z.D.M. Helena, A.C. Barana, Prediction of total nitrogen removal in a structured bed reactor for secondary and tertiary treatment of sanitary sewage, Desal. Water Treat., 126 (2018) 144–150.
[9] C. Ishigaki, H. Yamashita, A domestic wastewater purification tank for domestic and disposal wastewater, J. Environ. Conserv. Eng., 33 (2004) 671–675.
[10] H. Chen, A. Li, Q. Wang, D. Cui, C.W. Cui, F. Ma, Nitrogen removal performance and microbial community of an enhanced multistage A/O biofilm reactor treating low-strength domestic wastewater, Biodegradation, 29 (2018) 285–299.
[11] S.M. Monahan, V.S. Vitankar, R.O. Fox, CFD predictions for flow-regime transitions in bubble columns, AlChE J., 51 (2005) 1897–1923.
[12] E. Delnoij, J.A.M. Kuipers, W.P.M. van Swaaij, Computational fluid dynamics applied to gas–liquid contactors, Chem. Eng. Sci., 52 (1997) 3623–3638.
[13] A. Lapin, A. Lübbert, Numerical simulation of the dynamics of two-phase gas—liquid flows in bubble columns, Chem. Eng. Sci., 49 (1994) 3661–3674.
[14] A. Sokolichin, G. Eigenberger, Gas—liquid flow in bubble columns and loop reactors: Part I. Detailed modelling and numerical simulation, Chem. Eng. Sci., 49 (1994) 5735–5746.
[15] L. Díez, B.E. Zima, W. Kowalczyk, A. Delgado, Investigation of multiphase flow in sequencing batch reactor (SBR) by means of hybrid methods, Chem. Eng. Sci., 62 (2007) 1803–1813.

[16] B.E.Z. Kulisiewicz, L. Díez, W. Kowalczyk, C. Hartmann, A. Delgado, Biofluid mechanical investigations in sequencing batch reactor (SBR), Chem. Eng. Sci., 63 (2008) 599–608.
[17] X. Wang, J. Ding, N.Q. Ren, B.F. Liu, W.Q. Guo, CFD simulation of an expanded granular sludge bed (EGSB) reactor for biohydrogen production, Int. J. Hydrogen Energy, 34 (2009) 9686–9695.
[18] T.T. Ren, M. Yang, B.J. Ni, H.Q. Yu, Hydrodynamics of up-flow anaerobic sludge blanket reactors, AIChE J., 55 (2009) 516–528.
[19] S.P.o. China, Discharge Standard of Pollutants for Municipal Wastewater Treatment Plant, GB18918–2002, 2003.
[20] S. Lochmatter, G.G. Gil, C. Holliger, Optimized aeration strategies for nitrogen and phosphorus removal with aerobic granular sludge, Water Res., 47 (2013) 6187–6197.
[21] S. Cho, N. Fujii, T. Lee, S. Okabe, Development of a simultaneous partial nitrification and anaerobic ammonia oxidation process in a single reactor, Bioresour. Technol., 102 (2011) 652–659.
[22] E. Mohsenzadeh, M.K. Moraveji, R. Davarnejad, Influence of acetaminophen on gas hold-up, liquid circulation velocity and mass transfer coefficient in a split-cylinder airlift bioreactor, J. Mol. Liq., 173 (2012) 113–118.
[23] T.T. Devi, B. Kumar, Effects of superficial gas velocity on process dynamics in bioreactors, Thermophys. Aeromech., 21 (2014) 365–382.
[24] C. Zhong, Y. Wang, Y. Wang, J. Lv, Y. Li, J. Zhu, High-rate nitrogen removal and its behavior of granular sequence batch reactor under step-feed operational strategy, Bioresour. Technol., 134 (2013) 101–106.
[25] B. Wang, W. Wang, H.J. Han, H.B. Hu, H.F. Zhuang, Nitrogen removal and simultaneous nitrification and denitrification in a fluidized bed step-feed process, J. Environ. Sci., 24 (2012) 303–308.
[26] G.B. Zhu, Y.Z. Peng, S.Y. Wang, S.Y. Wu, B. Ma, Effect of influent flow rate distribution on the performance of step-feed biological nitrogen removal process, Chem. Eng. J., 131 (2007) 319–328.